ELSEVIER

Thermochimica Acta 254 (1995) 193–207

thermochimica acta

A kinetic study of the thermal decomposition of iron(III) hydroxide oxides. Part 1. α-FeO(OH) in banded iron formations

Nobuyoshi Koga *, Shigeru Takemoto, Syougo Okada, Haruhiko Tanaka

Chemistry Laboratory, Faculty of School Education, Hiroshima University, 3-1-33 Shinonome, Minami-Ku, Hiroshima 734, Japan

Received 7 June 1994; accepted 31 July 1994

Abstract

As the first part of a series on kinetic studies on the thermal decomposition of iron(III) hydroxide oxide, α-FeO(OH), involved in a crustal material, banded iron formations, is subjected to thermogravimetric measurements at various constant and linearly increasing temperatures. The validity of the kinetic procedures employed in a series of kinetic studies is tested by a comparative kinetic study of the thermal decomposition of α-FeO(OH) involved in two characteristic parts of banded iron formations, in which 54.9 ± 1.2 and 44.5 ± 2.3 wt% of α-FeO(OH) are involved. Under isothermal conditions, kinetic agreement with an Avrami–Erofe'ev equation A_m ($m \approx 1.5$) was observed for the thermal decomposition of both samples to α-Fe_2O_3. The Arrhenius parameters calculated for the two samples are identical within the statistical error. For linearly increasing temperatures, the apparent activation energies calculated for these samples by a different isoconversion method were different by about 35 kJ mol^{-1}. Kinetic agreement with $A_{1.5}$ for the sample containing 54.9 wt% of α-FeO(OH) was identical to that found under isothermic conditions. The kinetics of the other sample were characterized by the larger apparent Arrhenius parameters and the kinetic agreement with the A_1 law. The different kinetic behavior under non-isothermal conditions of the samples was probably due to the difference in diffusional removal of evolved water vapor, depending on the compositional difference in the two characteristic parts of banded iron formations.

Keywords: Coupled technique; Decompositon; Iron hydroxide oxide; Isothermal; Kinetics; Non-isothermal

* Corresponding author.

SSDI 0040-6031(94)02050-7

1. Introduction

Iron(III) oxides and hydroxide oxides are useful materials in many fields of industry. Methods of preparation of these materials under various conditions have been examined to control the morphology, particle size and its distribution, which are essential for attaining the desired physico-chemical properties [1–10]. Iron(III) hydroxide oxides are both the objective of the preparation and the precursor in preparing iron(III) oxides. The thermal decomposition of iron(III) hydroxide oxide is one of the most important processes in the preparation of iron(III) oxides. The decomposition kinetics may depend on the morphology, particle size and its distribution and control the physico-chemical properties of the product oxides. In the present series of kinetic studies of the thermal decomposition of iron(III) hydroxide oxides, effects of morphology, particle size and its distribution, which are controlled in preparation, on the kinetics of thermal decomposition are investigated through a systematic kinetic analysis of thermogravimetric curves. The finding of a relationship between the decomposition kinetics and morphology of the product oxides is also attempted. As the first part of the series of studies, α-FeO(OH) involved in a crustal material, banded iron formations (BIFs), is singled out as a reference for the subsequent kinetic studies on the thermal decomposition of synthetic iron(III) hydroxide oxides. An evaluation of the validity of the kinetic procedures employed in the present series of kinetic studies is also attempted.

Recently, a physico-chemical characterization of BIFs collected at Hemmersley in north-western Australia was reported through a comprehensive study of crystallographic, magnetic and thermoanalytical measurements [11]. The specimen shows a prominent layered or banded structure in shades of red and black, where the thickness of the respective bands are in the order of 10 mm. Both the bands are mainly composed of α-SiO_2, α-Fe_2O_3, γ-Fe_2O_3 and α-FeO(OH). The black band includes more γ-Fe_2O_3 than the red band. Mössbauer spectroscopy revealed that α-FeO(OH) exists as a finely dispersed powder.

2. Experimental

The red and black portions in the BIFs, from Hammersley in north-western Australia, were separated by a diamond saw and named BIFs(A) and BIFs(B), respectively. Each sample, crushed with a hammer and then pulverized finely with a pestle and mortar, was characterized by powder X-ray diffraction (XRD), FT-IR spectroscopy (IR) and thermogravimetry (TG). XRD patterns and IR spectra of the samples were obtained using Rigaku Miniflex with Fe Kα radiation filtered by Mn, and Shimadzu FT-IR by the diffuse reflectance method, respectively. Simultaneous measurements of TG-DTG were carried out using Shimadzu TGA-50 at a heating rate of 10 K min^{-1} under N_2 at a flow rate of 30 ml min^{-1}.

Systematic TG measurements were done on the above-described instrument, in order to characterize kinetically the thermal decomposition process of α-FeO(OH) involved in the samples. For BIFs(A) and (B), 5.0 and 6.0 mg of the samples were

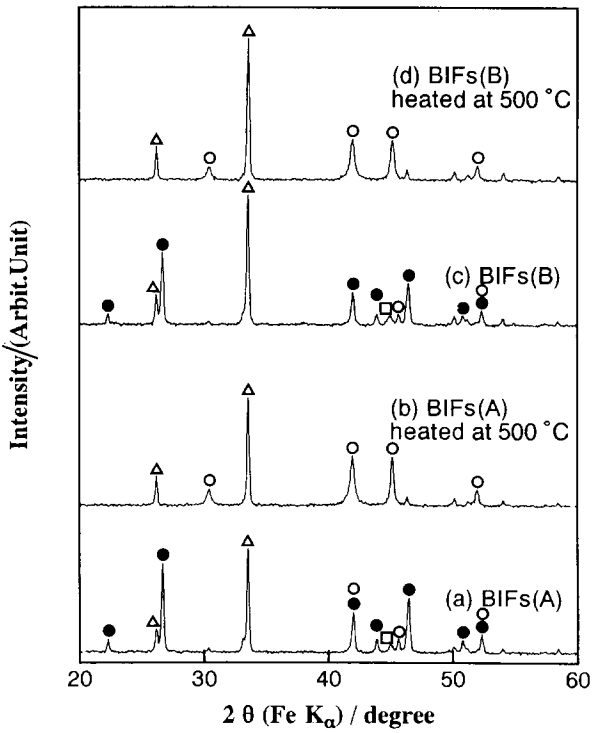

Fig. 1. Powder X-ray diffraction patterns for BIFs(A) and (B), at room temperature and 500°C: ●, α-FeO(OH); ○, α-Fe_2O_3; □, γ-Fe_2O_3 or Fe_3O_4; △, SiO_2.

weighed, respectively, on a platinum crucible, 5 mm in diameter and 2.5 mm in height, so that the mass loss due to the thermal decomposition in both samples was 0.27 mg. Isothermal mass-loss traces were obtained at various constant temperatures in the range 240–290°C in N_2 at a flow rate of 30 ml min^{-1}. Non-isothermal TG and DTG measurements were also carried out at various heating rates in the range 2.0–10.0 K min^{-1}, the conditions being otherwise identical with those for the isothermal runs.

3. Results and discussion

XRD patterns of BIFs(A) and (B) are shown in Fig. 1. Diffraction peaks corresponding to α-FeO(OH) are observed for both samples (see Fig. 1, curves (a) and (c)). Fig. 2 shows IR spectra of BIFs(A) and (B), where the absorption peaks at 3100, 904 and 774 cm^{-1} are characteristic of α-FeO(OH), being due to O–H stretching, O–H bending and Fe–O stretching vibrations, respectively. Inclusion of α-FeO(OH) in BIFs is characteristic of the present sample, different from that obtained from Ari Dongri, Central India [12]. Fig. 3 represents the typical TG and

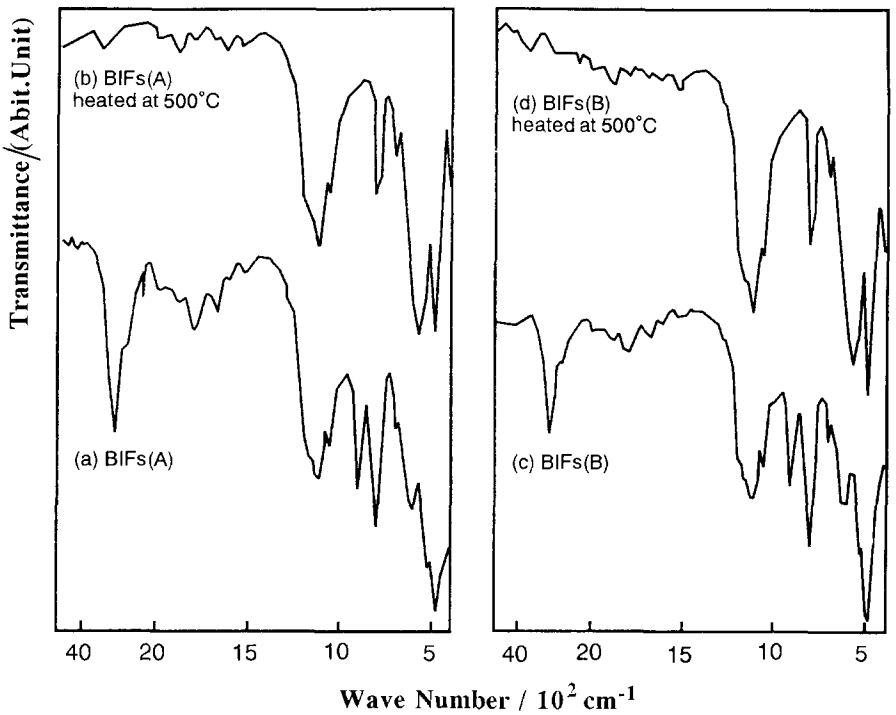

Fig. 2. IR spectra for BIFs(A) and (B), at room temperature and 500°C.

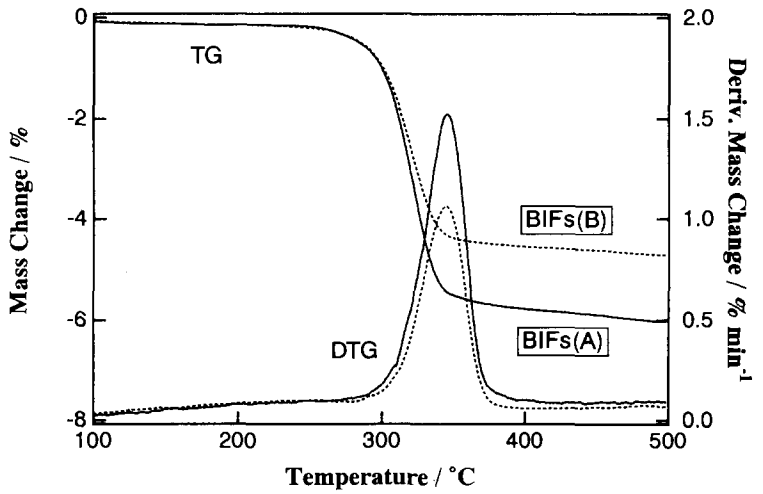

Fig. 3. Typical TG and DTG curves for the thermal decomposition of BIFs(A) and (B) at a heating rate of 10 K min^{-1}.

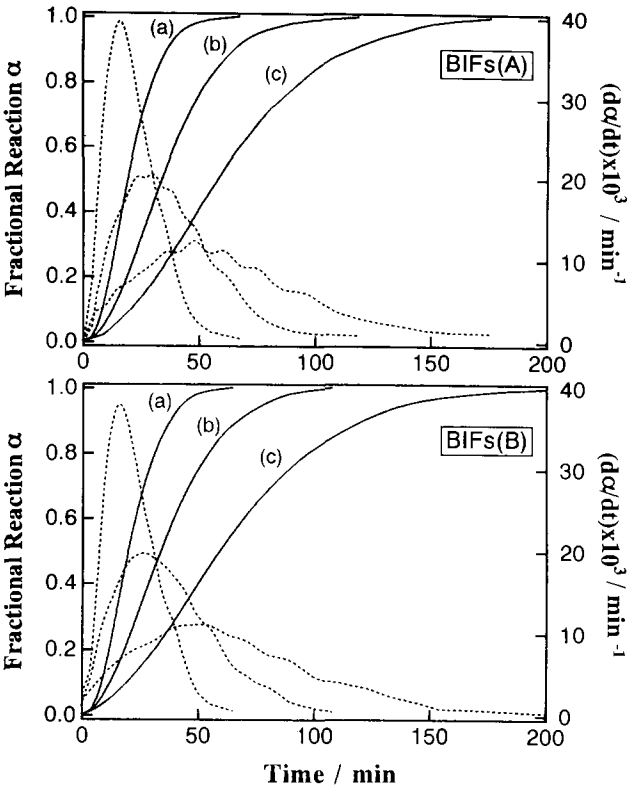

Fig. 4. Typical plots of α and $d\alpha/dt$ against t for BIFs(A) and (B) at various constant tempertures: (a) 280°C, (b) 270°C and (c) 260°C.

DTG curves for BIFs(A) and (B). We see that the well-defined single DTG peak appears at around 300°C for both samples, and BIFs(A) loses more mass than BIFs(B). XRD patterns and IR spectra of their decomposition products are shown in Figs. 1 and 3, respectively. The characteristic peak of α-FeO(OH) disappear in the decomposition products. Accordingly, the mass-loss process is identified as being due to the thermal decomposition of α-FeO(OH) involved in the samples: $2FeOOH \rightarrow Fe_2O_3 + H_2O$. The contents of α-FeO(OH) calculated from the degree of mass loss in the thermal decomposition were 54.85 ± 1.22 and 44.45 ± 2.23 wt% for BIFs(A) and (B), respectively.

3.1. Isothermal decomposition

Fig. 4 shows typical plots of fractional reaction α against t for both samples at various constant temperatures. The patterns are sigmoidal, indicating the nucleation and growth models as a possible reaction mechanism. The rate data were compared with the kinetic model functions $g(\alpha)$ through plots of $g(\alpha)$ against t assuming

Table 1
Kinetic model functions $f(\alpha)$ usually employed for the solid-state reactions, together with the integral forms $g(\alpha)$

Model	Symbol	$f(\alpha)$	$g(\alpha) = \int_0^\alpha \frac{d\alpha}{f(\alpha)}$
One-dimensional diffusion	D_1	$\frac{1}{2\alpha}$	α^2
Two-dimensional diffusion	D_2	$-\frac{1}{\ln(1-\alpha)}$	$\alpha + (1-\alpha)\ln(1-\alpha)$
Three-dimensional diffusion (Jander)	D_3	$\frac{3(1-\alpha)^{2/3}}{2[1-(1-\alpha)^{1/3}]}$	$[1-(1-\alpha)^{1/3}]^2$
Three-dimensional diffusion (Ginstring–Brounshtein)	D_4	$\frac{3}{2[(1-\alpha)^{1/3}-1]}$	$1-\frac{2\alpha}{3}-(1-\alpha)^{2/3}$
Phase boundary controlled	R_n $(1 \le n \le 3)$	$n(1-\alpha)^{1-1/n}$	$1-(1-\alpha)^{1/n}$
Nucleation and growth (Avrami–Erofe'ev)	A_m $(0.5 \le m \le 4)$	$m(1-\alpha)[-\ln(1-\alpha)]^{1-1/m}$	$[-\ln(1-\alpha)]^{1/m}$

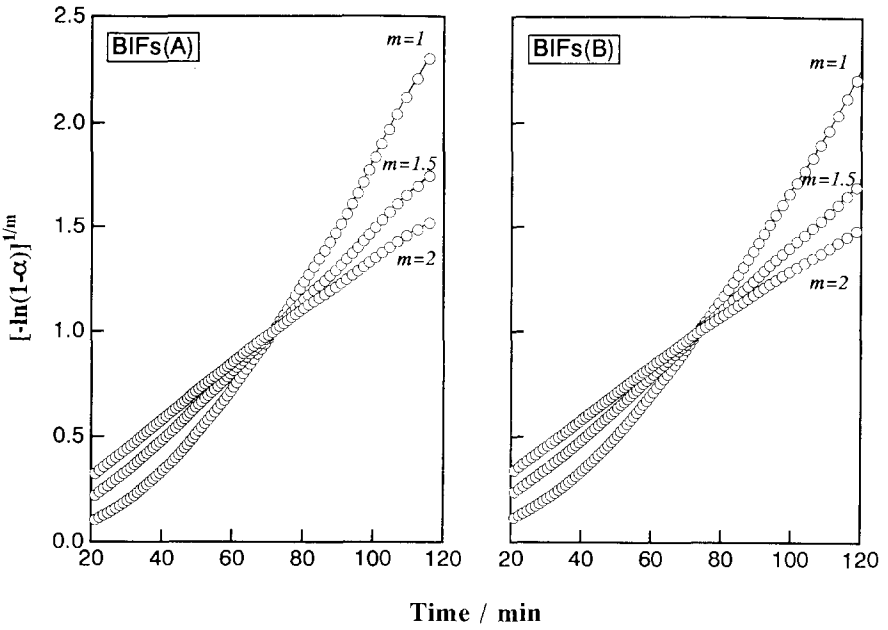

Fig. 5. Typical plots of $[-\ln(1-\alpha)]^{1/m}$ against t at 260°C for BIFs(A) and (B).

Table 2
The most appropriate non-integral kinetic exponent m in the A_m law, together with values of k

Temperature in °C	BIFs(A)			BIFs(B)		
	m	$k \times 10^4$ in s^{-1}	γ [a]	m	$k \times 10^4$ in s^{-1}	γ [a]
240	1.9	0.54	0.9999	–	–	–
245	1.5	0.95	0.9999	1.5	0.83	0.9998
250	1.6	1.35	0.9998	1.6	1.37	0.9999
255	–	–	–	1.5	1.86	0.9998
260	1.7	2.46	0.9998	1.6	2.40	0.9998
265	–	–	–	1.6	3.54	0.9999
270	1.8	4.34	0.9999	1.7	4.29	0.9999
275	–	–	–	1.6	6.13	0.9999
280	1.6	8.65	0.9999	1.5	8.72	0.9999
290	1.8	12.81	0.9999	–	–	–

[a] Correlation coefficient.

$$g(\alpha) = kt \tag{1}$$

Table 1 lists the kinetic model functions $g(\alpha)$ usually employed to characterize the kinetics of solid-state reactions, together with those in different forms $f(\alpha)$ [13,14]. Within $0.10 \leq \alpha \leq 0.90$, agreement with an Avrami–Erofe'ev (A_m) law,

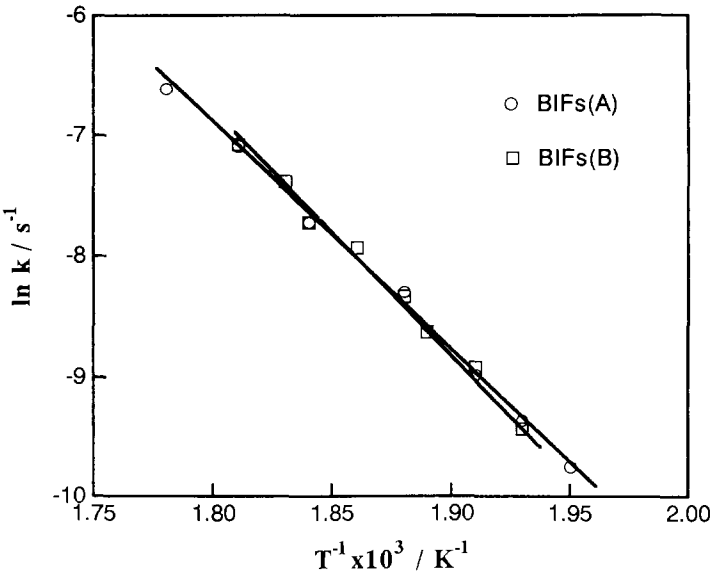

Fig. 6. Arrhenius plots assuming the non-integral kinetic exponents $m = 1.7$ and $m = 1.6$ in the A_m law for BIFs(A) and (B), respectively.

Table 3
The kinetic parameters, E and log A, for the thermal decomposition of BIFs(A) and (B) determined by assuming the non-integral kinetic exponent m in the A_m law

Sample	m	E in kJ mol^{-1}	log(A/s^{-1})	$-\gamma$ [a]
BIFs(A)	1.7 ± 0.2	154.5 ± 3.0	11.5 ± 0.3	0.9988
BIFs(B)	1.6 ± 0.1	159.0 ± 4.8	12.0 ± 0.5	0.9980

[a] Correlation coefficient.

$[-\ln(1-\alpha)]^{1/m} = kt$, with $m \leq 2$ was estimated through plots of the possible kinetic model functions, $g(\alpha)$, against t. Fig. 5 shows typical plots of $[-\ln(1-\alpha)]^{1/m}$ against t at 260°C for BIFs(A) and (B).

By scanning the value of m in the A_m law, the most appropriate non-integral values of m at the respective temperatures were determined from the linearity of the $[-\ln(1-\alpha)]^{1/m}$ vs. t plots. Table 2 lists the optimum value of m at the respective temperatures, together with the apparent rate constant k. Mean values of $m = 1.7 \pm 0.2$ and $m = 1.6 \pm 0.1$ were obtained for the BIFs(A) and (B), respectively, showing the same nominal kinetic obedience between the samples. Formally, the A_m law with $m \approx 1.5$ is interpreted as representing a nucleation and growth type mechanism, controlled by the diffusion process of three-dimensional growth of nuclei or by first order nucleation and its one-dimensional growth regulated by diffusion [13].

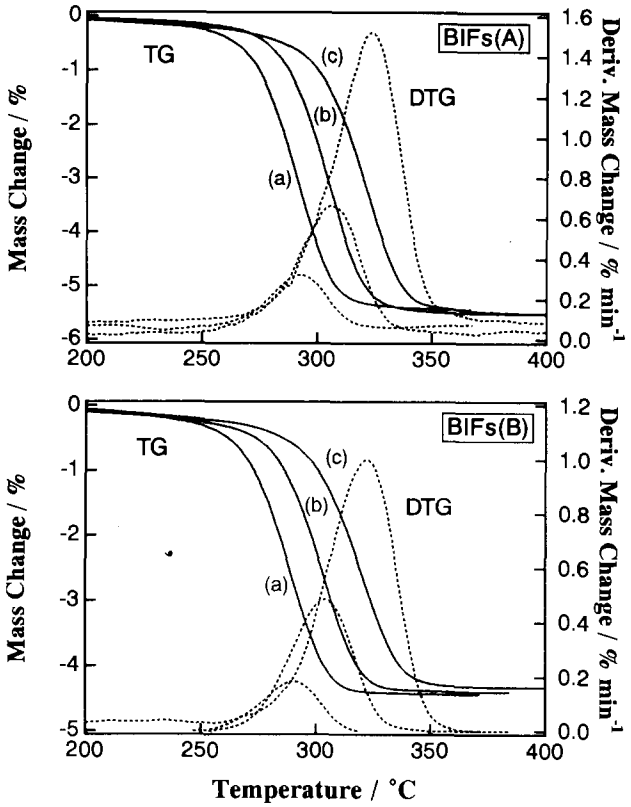

Fig. 7. Typical TG and DTG curves for the thermal decomposition of BIFs(A) and (B) at various heating rates: (a) 2, (b) 4 and 8 K min^{-1}.

Fig. 6 shows the Arrhenius plots for the k values calculated by assuming the mean values of m for the respective samples. The apparent Arrhenius parameters for the respective samples are listed in Table 3. The kinetic parameters of the samples are in good agreement. It is expected that under isothermic conditions the overall kinetics of the thermal decomposition is less influenced by the compositional difference in the different parts of BIFs.

3.2. Non-isothermal decomposition

Fig. 7 shows the non-isothermal TG and DTG curves at various heating rates ϕ for the respective samples. The values of E at various α are calculated by an isoconversion method of the extended Friedman treatment [15,16] assuming the general kinetic equation

$$\frac{d\alpha}{dT}\phi = \frac{d\alpha}{dt} = A \exp(-E/RT) f(\alpha) \tag{2}$$

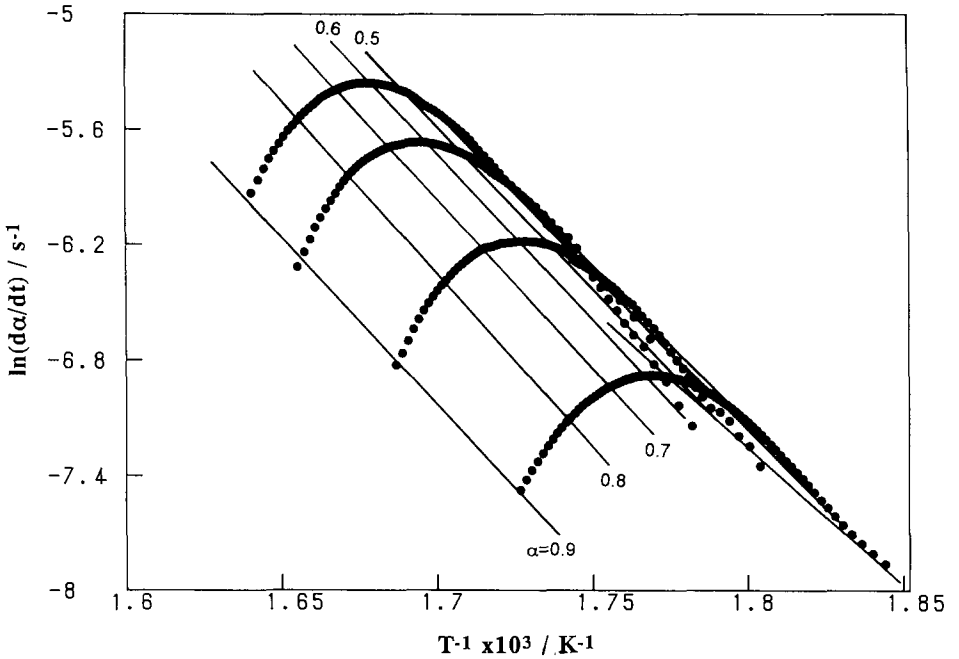

Fig. 8. Typical plots of $\ln(d\alpha/dt)$ against $1/T$ at various α from 0.1 to 0.9 in steps of 0.1 for BIFs(A).

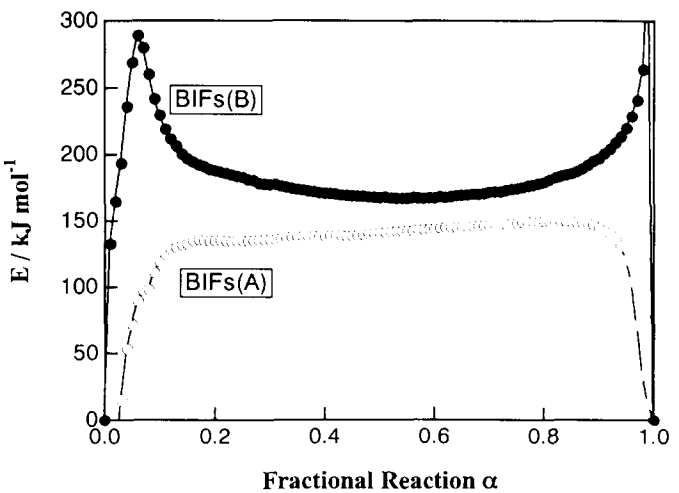

Fig. 9. α dependence of E values for BIFs(A) and (B).

where $f(\alpha)$ is the kinetic model function in differential form (see Table 1). By plotting $\ln[(d\alpha/dT)\phi]$ against $1/T$ at constant α, the apparent E values at the restricted α are obtained from the slope. Fig. 8 shows typical plots of $\ln(d\alpha/dt)$

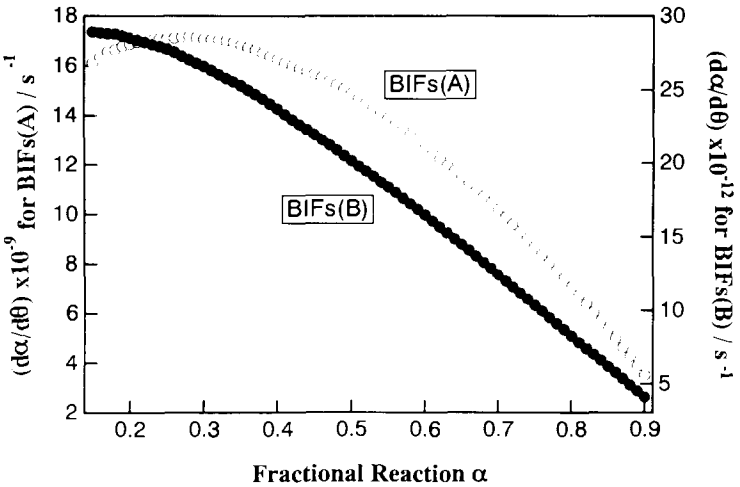

Fig. 10. α dependence of dα/dθ values for BIFs(A) and (B).

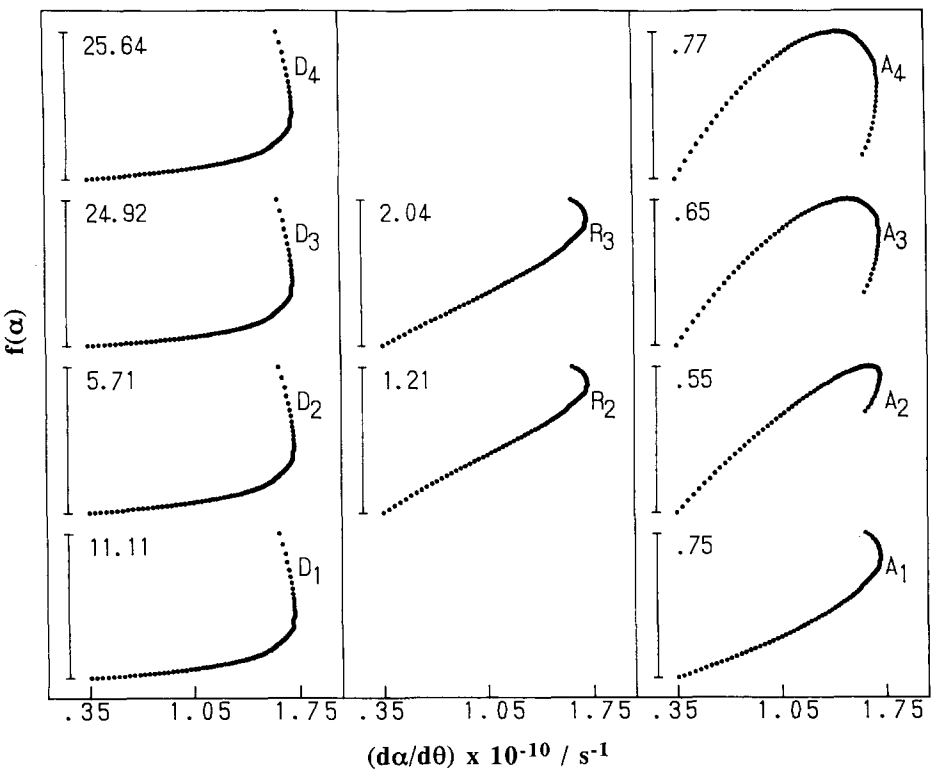

Fig. 11. Typical plots of various $f(\alpha)$ against $d\alpha/d\theta$ within the range $0.15 \leq \alpha \leq 0.90$ for BIFs(A).

against $1/T$ at various α for BIFs(A). The α dependence of the E values are shown in Fig. 9. The approximately constant value of E is observed in the range $0.15 \leq \alpha \leq 0.90$. This constancy is one of the pre-requisites for the subsequent kinetic analysis [17]. The mean values of E averaged over $0.15 \leq \alpha \leq 0.90$ were 142.0 ± 0.6 and 176.5 ± 1.0 kJ mol^{-1} for BIFs(A) and (B), respectively.

For the subsequent kinetic analysis, the generalized time θ [17,18] is introduced

$$\theta = \int_0^t \exp(-E/RT)\, dt \tag{3}$$

The first differentiation gives

$$\frac{d\theta}{dt} = \exp(-E/RT) \tag{4}$$

Combining Eq. (2) with Eq. (4) gives

$$\frac{d\alpha}{d\theta} = Af(\alpha) \tag{5}$$

The general kinetic equation is thus divided into enthalpy- and entropy-dependent terms [19], expressed by $d\theta/dt$ and $d\alpha/d\theta$, respectively.

$$\frac{d\alpha}{dt} = \frac{d\alpha}{d\theta}\frac{d\theta}{dt} \tag{6}$$

Using the mean value of E within $0.15 \leq \alpha \leq 0.90$, the values of $d\alpha/d\theta$ are determined from Eqs. (5) and (6). Fig. 10 shows the $d\alpha/d\theta$ vs. α plots for the respective samples. The patterns of these plots are slightly different for each of the samples. According to Eq. (5), the kinetic agreement with a particular $f(\alpha)$ was compared by plotting $f(\alpha)$ against $d\alpha/d\theta$. Fig. 11 shows the plots of ten possible $f(\alpha)$

Table 4
The most appropriate non-integral kinetic exponents in the empirical model functions $h(\alpha)$ for the non-isothermal decomposition of BIFs(A) and (B)

Symbol	$h(\alpha)$	BIFs(A)		BIFs(B)	
		Exponent	γ [a]	Exponent	γ [a]
D_L $(1 \leq L < 2)$	$\frac{1}{1-(1-\alpha)^{2/L-1}}$	$L = 1.9$	0.7243	$L = 1.9$	0.8523
D_L $(1 \leq L \leq 3)$	$\frac{L(1-\alpha)^{1-1/L}}{2[1-(1-\alpha)^{1/L}]}$	$L = 1.4$	0.7278	$L = 1.4$	0.8549
D_L $(2 \leq L \leq 3)$	$\frac{1}{(1-\alpha)^{2/L-1}-1}$	$L = 2.1$	0.7243	$L = 2.1$	0.8523
R_N $(1 \leq N \leq 3)$	$N(1-\alpha)^{1-1/N}$	$N = 1.1$	0.9885	$N = 2.6$	0.9984
A_M $(0.5 \leq M \leq 4)$	$M(1-\alpha)[-\ln(1-\alpha)]^{1-1/M}$	$M = 1.4$	0.9994	$M = 1.1$	0.9993

[a] Correlation coefficient.

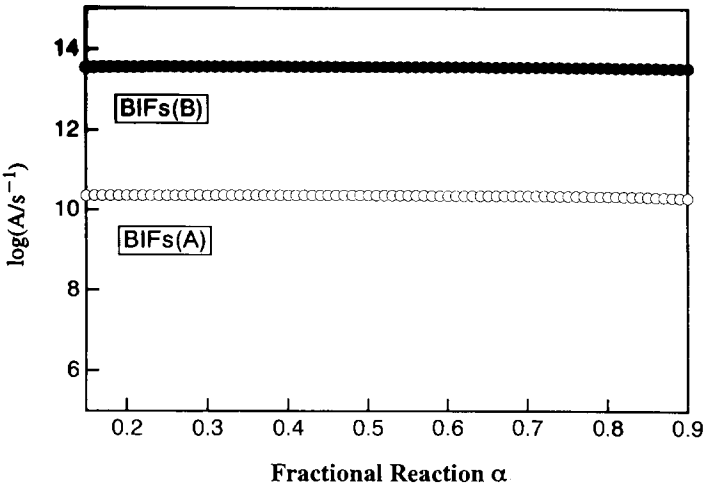

Fig. 12. α dependence of the values of $\log A$ for BIFs(A) and (B).

against $d\alpha/d\theta$ within $0.15 \leq \alpha \leq 0.90$ for BIFs(A). Linear dependence between the $f(\alpha)$ and $d\alpha/d\theta$ was not observed for $f(\alpha)$ with integral kinetic exponents.

Because the use of such inappropriate kinetic model functions leads to distortion of the other kinetic parameters as a simple mathematical consequence [20,21], the kinetic model function can be extended to the empirical kinetic model functions $h(\alpha)$ in order to obtain the best linearity of the plot. Introducing the accommodation function $a(\alpha)$ [22,23], $h(\alpha)$ is interpreted as the function accommodating the distortion of the actual reaction process from the idealized model $f(\alpha)$

$$h(\alpha) = f(\alpha)a(\alpha) \tag{7}$$

It is apparent, however, that $a(\alpha)$ is extremely difficult to formalize, based on real physical chemistry, and is possibly expressed by the empirical (analytical) formula [21,22]. One of the simplest examples of $h(\alpha)$ is the application of the non-integral kinetic exponent to $f(\alpha)$ as shown in Table 4 [23,24]. By changing the kinetic exponents in the respective $h(\alpha)$, the most appropriate kinetic exponents were determined from the linearity of the $h(\alpha)$ vs. $d\alpha/d\theta$ plots. Table 4 lists the most appropriate non-integral values of kinetic exponents in the respective $h(\alpha)$, together with the correlation coefficients of the linear regression analysis. Although the kinetic agreement with the A_M laws was estimated as in the case of isothermal decomposition, the different kinetic exponents $M = 1.4$ and $M = 1.1$ were obtained for BIFs(A) and (B), respectively. Using such $h(\alpha)$, the pre-exponential factors A at various α were calculated in terms of Eq. (5). Fig. 12 shows the α dependence of the logarithmic pre-exponential factor $\log A$. For the respective samples, the values of A are approximately constant irrespective of α, with average values of $\log(A/s^{-1}) = 10.36 \pm 0.02$ and 13.57 ± 0.02. The constancy of the A values at various α, a pre-requisite of the general kinetic equation [19], suggests that the kinetic treatments carried out for the present reactions were appropriate [25].

The difference in the kinetic parameters for the non-isothermal decomposition of BIFs(A) and (B) seems to be due to the compositional difference, e.g. the different content of α-FeO(OH), as well as the constructive difference in the respective portions in the BIFs. For BIFs(A) containing less α-FeO(OH), the gross diffusion of the evolved water vapor becomes difficult compared with that of BIFs(A), especially when the decomposition rate is relatively high, i.e. under non-isothermal conditions at higher heating rates. The overall kinetics are then influenced by the higher partial pressure of the evolved water vapor. This interpretation is supported by the interpretation of the A_1 law, in which the reaction is controlled by the diffusional removal of the evolved water vapor through the sample matrix of finely dispersed powders [26].

4. Conclusions

α-FeO(OH) involved in the banded iron formations decomposes to α-Fe_2O_3 and water vapor at around 250–350°C. The process is well characterized kinetically by the Avrami–Erofe'ev A_m law with $m < 2$, in which the mechanism is interpreted formally as a nucleation and growth type controlled by the diffusion process of three-dimensional growth of nuclei or by first order nucleation and its one-dimensional growth regulated by diffusion. The detectable changes in the kinetic exponent and the Arrhenius parameters are observed depending on the sample and measuring conditions. Physico-chemical interpretations of such variations in the overall kinetics are to be made in such a series of TA kinetic studies, through complementary kinetic approaches and other physico-chemical measurements.

The present kinetic procedure for non-isothermal decomposition is more reliable than the conventional procedure, because of the check system on the constancy of the Arrhenius parameters during the reaction.

References

[1] G. Okamoto, R. Furuichi and N. Sato, Electrochim. Acta, 12 (1986) 1287.
[2] T. Ishikawa and K. Inouye, Bull. Chem. Soc. Jpn., 45 (1972) 2350; 46 (1973) 2665; 48 (1975) 1580.
[3] M. Kiyama and T. Takada, Bull. Chem. Soc. Jpn., 46 (1973) 1680.
[4] M. Kiyama, S. Shamoto, N. Horiishi, Y. Okuda and T. Takada, Bull. Inst. Chem., 64 (1986) 150.
[5] K.M. Parida, J. Mater. Sci., 23 (1988) 1201.
[6] S. Hamada, Y. Kudo and T. Matsumoto, Bull. Chem. Soc. Jpn., 62 (1989) 1017.
[7] K. Kandori, M. Fukuoka and T. Ishikawa, J. Mater. Sci., 26 (1991) 3313.
[8] T. Ishikawa, T. Takeda and K. Kandori, J. Mater. Sci., 27 (1992) 4537.
[9] M. Kiyama, T. Kurata, T. Nakamura and T. Takada, Bull. Inst. Chem. Res. Kyoto Univ., 68 (1991) 275.
[10] T. Asai, K. Ado and O. Nakamura, Chem. Exp., 6 (1991) 355 (in Japanese); Shikizai, 65 (1992) 68 (in Japanese).
[11] T. Tsutaoka, N. Koga, M. Suzuki and T. Hayashi, Bull. Fac. Sch. Educ. Hiroshima Univ., Part II, 16 (1994) 79.
[12] D. Das, M.B. Chakraborti, K. Choudhury, P.M.G. Nambissan, B.R.S. Babu, P. Sen, Sangeeta and C.K. Majumdar, Bull. Mater. Sci., 15 (1992) 161.

[13] M.E. Brown, D. Dollimore and A.K. Galwey, in C.H. Bamford and C.F.H. Tipper (Eds.), Comprehensive Chemical Kinetics, Vol. 22, Reactions in the Solid State, Elsevier, Amsterdam, 1980.
[14] J. Sestak, in G. Svehla (Ed.), Comprehensive Analytical Chemistry, Vol. 12, Part D, Thermophysical Properties of Solids, Their Measurements and Theoretical Thermal Analysis, Elsevier, Amsterdam, 1984.
[15] H.L. Friedman, J. Polym. Sci. C, 6 (1964) 183.
[16] T. Ozawa, J. Therm. Anal., 3 (1986) 547.
[17] T. Ozawa, Bull. Chem. Soc. Jpn., 38 (1965) 1881.
[18] T. Ozawa, Thermochim. Acta, 100 (1986) 109.
[19] K. Koga and H. Tanaka, Thermochim. Acta, 224 (1993) 141.
[20] N. Koga, J. Sestak and J. Malek, Thermochim. Acta, 188 (1991) 333.
[21] N. Koga, J. Malek, J. Sestak and H. Tanaka, Netsu Sokutei, 20 (1993) 210.
[22] J. Sestak, J. Therm. Anal., 36 (1990) 1997.
[23] N. Koga and H. Tanaka, J. Therm. Anal., 41 (1994) 455.
[24] R. Ozao and M. Ochiai, J. Ceram. Soc. Jpn., 101 (1993) 263.
[25] N. Koga, Thermochim. Acta, 244 (1994) 1.
[26] V.B. Oknotnikov, React. Kinet. Catal. Lett., 38 (1989) 359.